Numerical Analysis of Laminar Flow in a Double-Walled Annular Heat Pipe

Amir Faghri* and Shahram Parvani†
Wright State University, Dayton, Ohio

The parabolic and elliptic representations of the governing equations of fluid motion for steady two-dimensional laminar flow in a double-walled annular heat pipe with various distributions of heating and cooling loads have been analyzed numerically. The results show that the flow reverses at very high condensation rates and that the parabolic representation provides a sufficiently accurate picture of the vapor pressure variations at both low and high evaporation and condensation rates. An approximate analytical method is also presented that can predict the pressure drop and velocity variation accurately along the double-walled annular heat pipe, as well as the location at which the flow reverses in the condenser zone.

Nomenclature

A = constant used in Eq. 13, $(1-K^2)/\ell n\ 1/K$
B = constant used in defining C, $(1-K^4)/(1-K^2)$
C = constant used in Eq. 13, $4(|Re_{I,E}| + |Re_{O,E}|)/(B-A)(1-K^2)$
C' = constant used in Eq. 15, $4(|Re_{I,C}| + |Re_{O,C}|)/(B-A)(1-K^2)$
D = constant used in Eq. 15, $2/(B-A)$
DI, DO = inner and outer pipe diameter, respectively
h_{fg} = latent heat of vaporization
K = ratio of inner radius to outer radius
LA, LC = length of the adiabatic and condenser sections, respectively
LE = length of the evaporator section
LT = total length of the heat pipe
P = vapor pressure
P^+ = normalized pressure, $(P-P_e)/\rho(w_{A,m})^2$
Q = heat-transfer rate per unit length
r = radial coordinate
R^+ = normalized radial distance, r/RO
RI, RO = inner and outer radii, respectively
Re = radial Reynolds number
$Re_{I,E}$ = inner wall radial Re in evaporator, $(RI)(V_{I,E})/\nu$
$Re_{I,C}$ = inner wall radial Re in condenser, $(RI)(V_{I,C})/\nu$
$Re_{O,E}$ = outer wall radial Re in evaporator, $(RO)(V_{O,E})/\nu$
$Re_{O,C}$ = outer wall radial Re in condenser, $(RO)(V_{O,C})/\nu$
Re_z = axial Reynolds number
v = radial component of the vapor velocity
v^* = dimensionless radial velocity, $v\ RO/\nu$
$V_{I,E}, V_{O,E}$ = blowing velocity at inner and outer walls, respectively, in evaporator
$V_{I,C}, V_{O,C}$ = suction velocity at inner and outer walls, respectively, in condenser
$V_{I,W}, V_{O,W}$ = radial velocity at inner and outer walls, respectively
w = axial component of the vapor velocity
$w_{A,m}$ = mean axial velocity in adiabatic section
$w_{z,m}$ = local mean axial velocity
$w^*_{z,m}$ = dimensionless local mean axial velocity, $w_{z,m}/w_{A,m}$
W^+ = normalized axial velocity, $w/w_{z,m}$
w^* = dimensionless axial velocity, $w/w_{A,m}$
z = axial coordinate
Z^+ = normalized axial coordinate, z/LT
z^* = dimensionless axial coordinate, $z\nu/(w_{A,m})(RO^2)$
μ = fluid absolute viscosity
ν = kinematic viscosity
ρ = fluid density

Subscripts
A = adiabatic section
C = condenser section
e = entrance of evaporator section
E = evaporator section
I = inner wall
O = outer wall
m = mixed-mean
R = flow has reversed
W = at the wall
z = at any z location

Received Nov. 3, 1986; revision received Aug. 5, 1987.

*Professor, Dept. of Mechanical Systems Engineering. Senior Member AIAA.
†Graduate Student, Dept. of Mechanical Systems Engineering.

Introduction

HEAT pipes, because of their great reliability and ability to transfer large amounts of heat, have been used in many fields of engineering. In many cases requiring heat pipes, the process is carried out at comparatively low temperatures, where the heat-transfer agent is a low boiling point liquid such as water or ethanol and the vapor flow in all sections of the heat pipe is laminar. In determining the heat capacity transmitted through the heat pipe, it is necessary to know the vapor pressure losses in the separate segments of the heat pipe. The evaporator and condenser sections can be considered to be pipes with porous walls, through which blowing and suction of vapor occurs. The end caps and the walls of the adiabatic section are impermeable.

Many investigators[1-11] have examined the problem of vapor flow in porous pipes and conventional heat pipes using numerical and analytical methods. Analysis of these theoretical and experimental investigations shows that approximate solutions of the Navier-Stokes equations using similarity analysis over the length of the condenser region for conventional heat pipes is valid for radial Reynolds numbers in the regions $0 < Re < 2.3$ and $Re > 9.1$.[8,9] In contrast to the

condenser section, similarity solutions have been found to exist for all values of the radial Reynolds number in the evaporator section. Numerical solutions of the complete governing equations of motion for conventional heat pipes were also considered by Refs. 8, 10, and 11. There is a disagreement among the investigators,[10,11] however, on the validity of the usage of the parabolic version of the equations of motion for the prediction of the vapor pressure drop in conventional heat pipes.

In this paper, an analysis is made concerning the vapor flow characteristics of a new high-capacity heat pipe, whcih is the double-walled annular heat pipe.[13] The double-walled annular heat pipe is made of two concentric pipes with unequal diameters. The pipe with a smaller diameter is placed inside the pipe with a larger diameter, and the pipes are sealed together with end caps, creating an annular vapor space. Wick structures can be placed on both the inner surface of the outer pipe and the outer surface of the inner pipe. The interior of the inner pipe is open to the surroundings. The heat transport capacity of the double-walled annular heat pipe will be much higher than that of conventional heat pipes as a result of an increase in capillary pressure as well as an increase in surface area exposed for the transfer of heat into and out of the pipe.[13]

Faghri[12] analyzed the two-dimensional, steady and incompressible vapor flow in a double-walled annular heat pipe, with water as the working fluid. The fully parabolic representation of the governing equations of motion was used for the solution of the vapor flow in the evaporator, adiabatic, and condenser sections of the heat pipe. The solutions for the evaporator, adiabatic, and condenser sections were obtained independently of each other. This was possible by assuming zero axial inlet velocity at the evaporator inlet and a fully developed profile at the inlet of the adiabatic and condenser sections. Because of these assumptions, an implicit, marching finite-difference method was possible.

The purpose of this work is to describe the computational procedure and the numerical solutions of the nonlinear differential elliptic equations of motion over the entire vapor flow domain of a double-walled annular heat pipe in order to allow all of the features of laminar flow to be taken into account. This was done to check the validity of the assumption made in Ref. 12. Also, the boundary-layer approximation was used in Ref. 12 for an elliptic problem. The validity of this approximation in the case of a significant vapor pressure drop in the double-walled annular heat pipe will be addressed. These numerical calculations are laborious and require a large amount of computer time. In view of this, an approximate analytical method is also presented to predict the change in static pressure and the velocity profiles of the vapor flow in all of the segments of the double-walled annular heat pipe. The analytical solution was found to predict the numerical results of the full Navier-Stokes equations to within 7%.

Mathematical Description

The physical problem under consideration is a right circular cylindrical annular cavity, as shown in Fig. 1. It is assumed that the vapor flow in all of the segments of the double-walled annular heat pipe, the evaporator, adiabatic, and the condenser sections, is operating under laminar, subsonic, and steady conditions and that the properties of the fluid are constant. Uniform radial inflow and outflow boundary conditions are used to model evaporation and condensation. Since the annulus is closed at both ends, it is required that the fluid that enters in the evaporator segment flows out through the condenser section. The differential equations associated with this axisymmetric problem are the continuity and the momentum equations, as follows in cylindrical coordinates.

$$\frac{\partial(\rho w)}{\partial z} + \frac{1}{r}\frac{\partial(\rho r v)}{\partial r} = 0 \tag{1}$$

$$w\frac{\partial(\rho w)}{\partial z} + v\frac{\partial(\rho w)}{\partial r} = -\frac{\partial P}{\partial z} + \mu\left[\left\{\frac{\partial^2 w}{\partial z^2}\right\} + \frac{1}{r}\frac{\partial w}{\partial r} + \frac{\partial^2 w}{\partial r^2}\right] \tag{2}$$

$$w\frac{\partial(\rho v)}{\partial z} + v\frac{\partial(\rho v)}{\partial r} = -\frac{\partial P}{\partial r} + \mu\left[\left\{\frac{\partial^2 v}{\partial z^2}\right\} + \frac{1}{r}\frac{\partial v}{\partial r} + \frac{\partial^2 v}{\partial r^2}\right] \tag{3}$$

It should be noted that, in Eq. (2) and (3), the terms in braces are associated with axial diffusion terms. These terms were neglected when the partially parabolic version was considered but were accounted for in the elliptic case. It should be emphasized that the partially parabolic scheme corresponds to the case in which only the axial diffusion terms are neglected and Eqs. (1)-(3) are solved simultaneously. Faghri[12] used the fully parabolic method in which the momentum equation in the radial direction (3) is also omitted.

The boundary conditions are defined as follows:

$$w(0,r) = v(0,r) = 0$$

$$w(LT,r) = v(LT,r) = 0$$

$$w(z,RI) = w(z,RO) = 0$$

$$v(z,RI) = V_{I,W}(z)$$

$$v(z,RO) = V_{0,W}(z)$$

$$P\left(0, \frac{RI + RO}{2}\right) = 0 \tag{4}$$

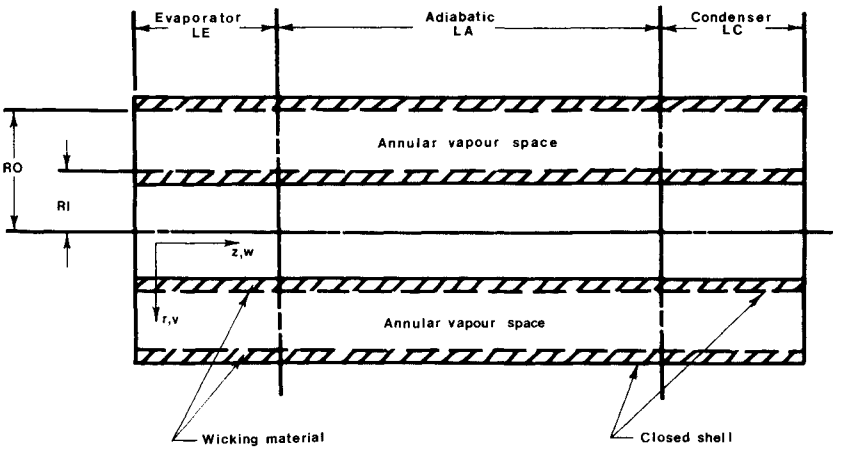

Fig. 1 Double-walled annular heat pipe and coordinate system.

The radial blowing and suction velocities at the inner and outer walls are taken to be uniform over the heating or cooling lengths and are related to the local heat rate per unit length by the following relations:

$$V_{O,E} = \frac{Q_{O,E}}{\pi DO \rho h_{fg}}$$

$$V_{I,E} = \frac{Q_{I,E}}{\pi DI \rho h_{fg}}$$

$$V_{O,C} = \frac{Q_{O,C}}{\pi DO \rho h_{fg}}$$

$$V_{I,C} = \frac{Q_{I,C}}{\pi DI \rho h_{fg}}$$

$$V_{I,A} = V_{O,A} = 0 \tag{5}$$

Solution Procedure

The finite-difference iteration method of solution developed by Spalding et al.,[14-15] which is employed in the generalized PHOENICS Computational Code,[16] was used for the elliptic and partially parabolic solutions of Eqs. (1)-(3), subject to the boundary conditions in Eq. (4). By this method, Eqs. (1-4) were solved using the finite-domain method outlined in Refs. 14 and 15. Finite-domain equations are derived by the integration of the differential equations over a control volume surrounding a grid node. The integrated source term is linearized, and the upwind differencing scheme is used in the convective terms in order to enhance numerical stability. Special care was taken to obtain results independent of the number of grids due to the use of the upwind differencing scheme. The SIMPLEST Practice[15] was used for solving the momentum equation rather than the well-established SIMPLE algorithm[17] in order to accelerate the convergence.

The equations for the radial and axial velocities were solved by a line-by-line method, which is similar to Stone's strongly implicit method but is free from parameters requiring case to case adjustment; the line-by-line method is less complex and takes less computer time. The pressure correction equation was solved by a whole-field method. Further details may be found in Ref. 18.

A converged solution was defined as the condition that obtains the difference between the absolute values of a dependent variable between two successive sweeps was less than 10^{-4} and the sum of the absolute volumetric error over the whole field was insignificant at 10^{-6} or less. Convergence was found to be affected by the radial Reynolds number at the walls. Therefore, the cases with high radial Reynolds numbers required more sweeps than the cases with lower radial Reynolds number. To improve convergence, a false time-step relaxation proportional to the fluid residence time in a typical cell was used. A convenient guideline for the setting of the underrelaxation factor for the velocities is to start with the minimum cell residence time, which is equal to the minimum cell width divided by the maximum velocity. In most cases, 200 sweeps were found to be adequate for convergence.

For the elliptic solution, the integration and marching proceeded along the axis of the annulus from $z = 0$ to $z = LT$. The solution exhibited good numerical stability and a fairly rapid rate of convergence of the iterative procedure. The accuracy of the numerical solution was checked in two ways:

1) The grid spacing was systematically varied and the results for different grid sizes were compared to the extrapolated results of infinitesimal grid spacing. Initial investigations were performed with a mesh with 20 cells in the radial direction and 40 cells in the axial direction. This was found to be adequate for low radial Reynolds numbers at the walls. A mesh with 40 cells in the radial direction and 80 cells in the axial direction was used for all of the results reported in this paper. The maximum deviation of the solution due to the refinement of the grid was 0.7% and, therefore, it was concluded that the results are practically independent of the number of cells in the mesh.

2) The numerical results were compared with known similar solutions[12] that exist for the fully parabolic version by solving each of the different segments of heat pipe independently.

Numerical Results and Discussion

The numerical analysis was performed for the flow of vapor in a double-walled annular heat pipe with a total length of 1 m and evaporator and condenser lengths each of 0.2 m; water at 100°C was used. The inner and outer diameters of the pipe were 0.0297 and 0.0456 m, respectively. The pipe dimensions were chosen close to the dimensions of an experimental double-walled annular heat pipe.[13]

The double-walled annular heat pipe performance was analyzed for a combination of symmetrical and asymmetrical blowing and suction conditions. Symmetrical blowing/suction is the condition in which blowing/suction velocities at both the inner and outer walls of the evaporator/condenser section are the same. Asymmetrical conditions occur when the blowing/suction velocities at the two walls are different from each other. Symmetrical blowing or suction does not correspond to symmetrical heating or cooling.

In order to investigate the accuracy and reliability of the numerical results obtained from the present analysis, the double-walled annular heat pipe was studied with the same radial Reynolds number and radius ratio (K) values as one of the cases studied by Faghri.[12] In his study, Faghri employed the boundary-layer approximation and analyzed the vapor flow in the evaporator and condenser sections independently. The present method solved the equations of motion of the vapor flow in the double-walled annular heat pipe as one domain all along the heat pipe.

Figure 2 presents the normalized pressure distribution P^+ along the heat pipe for the case with $K = 0.2$. The evaporator radial Reynolds numbers at the inner and outer walls are 0.6 and -3.0, respectively. The condenser radial Reynolds number at the inner wall is -0.6, whereas the radial Reynold number at the outer wall is 3.0. The pressure drop results obtained from the present analysis are within 1% of those obtained by Faghri.[12]

Figure 3 presents the normalized pressure drop P^+ distribution for the case with $K = 0.8$ and the radial Reynolds number at the inner wall in both the evaporator and condenser sections equal to 2.4. The radial Reynolds number at the outer wall in both the evaporator and condenser is set at 3.0. This case shows a deviation of 7% between Faghri's results[12] and those obtained from the present analysis. This is due to the fully parabolic scheme used in Ref. 12. The largest pressure drop along the heat pipe is observed for this case.

Figures 2 and 3 also demonstrate the normalized axial velocity profiles for the cases with $K = 0.2$ and 0.8, respectively. The axial velocity profile becomes fully developed in a short distance and stays parabolic all along the heat pipe for both cases.

Six distinct cases as listed in Table 1, were considered for the present analysis with $K = 0.65$. In each case, by assuming uniform blowing or suction velocities, the heating and cooling rates were considered to be uniform in the evaporator and condenser sections. The radial Reynolds numbers at the walls and the axial Reynolds number at the center of the adiabatic section are reported in Table 1. The overall mass balance was satisfied as well. Case 1 presents the analysis of viscous flow, meaning that the radial Reynolds numbers in the evaporator section are much smaller than 1, namely, 0.01 at both the inner and outer walls. Case 2 is an intermediate stage between case 1 and the other cases. In case 2, the radial Reynolds numbers in the evaporator and condenser sections are approximately 4. Cases 3-6 are cases in which the radial Reynolds numbers are much greater than 1. For all of the

cases mentioned, the normalized axial pressure variation and the radial variation of the normalized axial velocity are presented based on the numerical results obtained by the elliptic representation of the governing equation, with 40 grids in the radial direction and 80 grids in the axial direction. For cases 1-3, the partially parabolic representation of the governing equations was also used to obtain the numerical results. For all six cases, the axial pressure distribution of the heat pipe was calculated at three different locations; the inner wall, the centerline (which is at the midpoint between the two walls), and the outer wall. In each of the six cases, the three pressure distribution curves coincided all along the heat pipe, which confirmed that the radial pressure variation is negligible.

Figure 4 presents the normalized axial pressure drop P^+ along the heat pipe under the conditions of case 1. There is a continuous pressure drop along the heat pipe. The pressure drop in the adiabatic section is a straight line, whereas the pressure drop profile in the evaporator demonstrates the effects of the pressure head absorbed by evaporation. The pressure drop reaches a steady value at the condenser section, but there is no pressure recovery at that point. The overall pressure drop trend along the heat pipe is very close to the prediction of the pressure drop distribution by Tien et al.[10] for a conventional heat pipe. The drastic pressure drop along the heat pipe is caused by the shear stresses at both the inner and outer walls.

Figure 4 also shows the comparison of the normalized pressure drop profiles obtained by the elliptic and partially parabolic methods for case 1. This graph indicates that the partially parabolic results are within 4% of those obtained by the elliptic method. This means that the boundary-layer approximation provides sufficiently accurate results for the heating and cooling conditions of case 1.

As for the radial variation of the axial velocity for case 1, if we employ the elliptic method of solution, Fig. 4 shows that the radial profile of the normalized axial velocity stays parabolic all along the heat pipe. The same parabolic velocity profile along the heat pipe was also obtained by Bankston et al.[8] for conventional heat pipes with a small radial Reynolds number. It is obvious that vapor flow becomes fully developed at $Z^+ = 0.019$ in the evaporator section. Also, the axial velocity stays positive throughout the heat pipe, indicating that there is no region where the flow reverses under the cooling conditions of case 1.

Figure 5 presents the normalized axial pressure drop P^+ along the heat pipe for case 2. In this case, the radial Reynolds numbers at both the inner and outer walls were 4. As in case 1, there is a drastic pressure drop along the heat pipe. The pressure drop along the evaporator is increasing rapidly as a result of the increase in the axial momentum. The pressure drop along the adiabatic section is increasing as a linear function of the axial distance. In the condenser, the pressure drop becomes steady, but there is no pressure recovery observed. This is due to the loss of axial momentum by the flow through the heat pipe. For case 2, the nondimensional pressure drop distribution obtained using the elliptic method of solution differs less than 0.3% from that of the partially parabolic method of solution. Therefore, the partially parabolic method provides an accurate approximation for this case.

Figure 5 also presents the radial profiles of the normalized axial velocity W^+ for case 2. For this case, with the radial Reynolds numbers equal to 4, the axial velocity profile has changed very little compared to the axial velocity profile obtained for the radial Reynolds numbers equal to 0.01 of case 1. The axial velocity becomes fully developed at $Z^+ = 0.019$. Furthermore, the velocity maintains a parabolic profile throughout the annulus. There is no region where the flow reverses in any part of the condenser section under the cooling conditions of case 2. The axial velocity profiles of case 2, as well as the axial velocity profiles given for case 1, indicate the possibility of using similarity solutions to obtain analytical results for cases 1 and 2.

Figure 6 presents the normalized axial pressure drop P^+ along the heat pipe for case 3, where the radial Reynolds

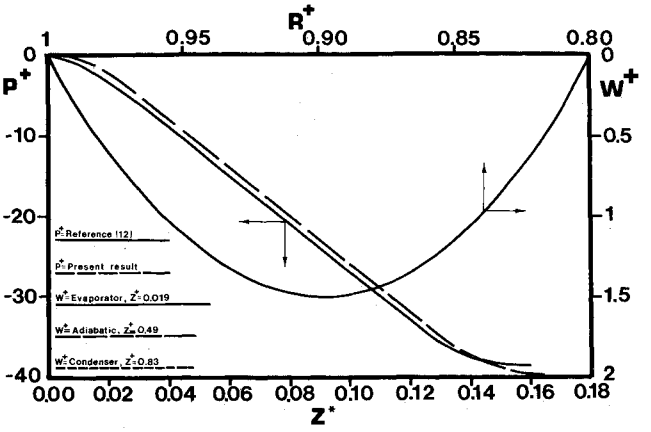

Fig. 3 Normalized pressure distribution and radial variation of the normalized axial velocity along the heat pipe with $K = 0.8$ evaporator *Re*, inner wall = 2.4, outer wall = − 3.0, condenser *Re*, inner wall = − 2.4, outer wall = 3.0.

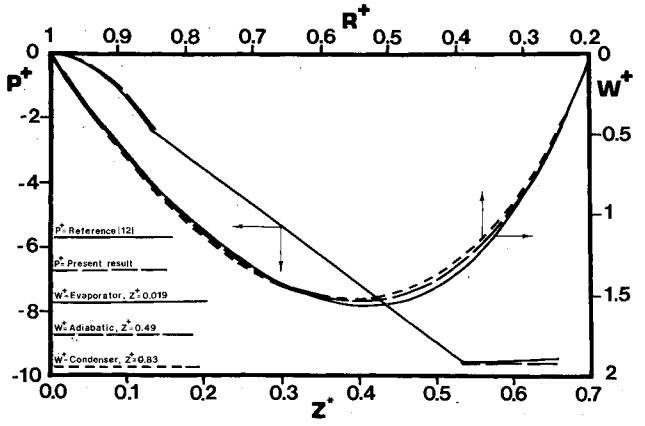

Fig. 2 Normalized pressure distribution and radial variation of the normalized axial velocity along the heat pipe with $K = 0.2$ evaporator *Re*, inner wall = 0.6, outer wall = − 3.0, condenser *Re*, inner wall = − 0.6, outer wall = 3.0.

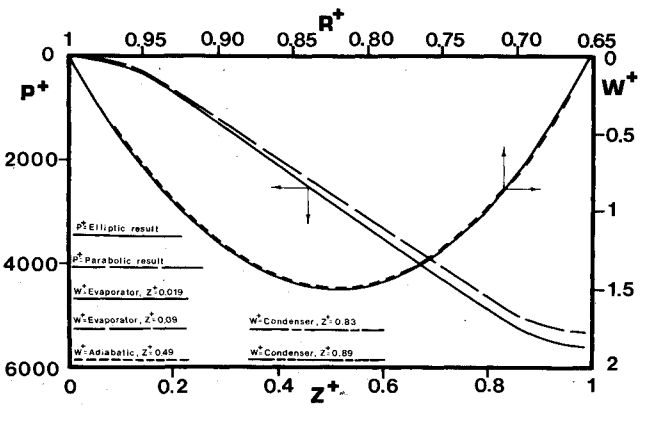

Fig. 4 Comparison of the elliptic and parabolic normalized pressure drop and radial variation of the normalized axial velocity along the heat pipe with $K = 0.65$ evaporator *Re*, at both walls = 0.01, condenser *Re*, at both walls = 0.01.

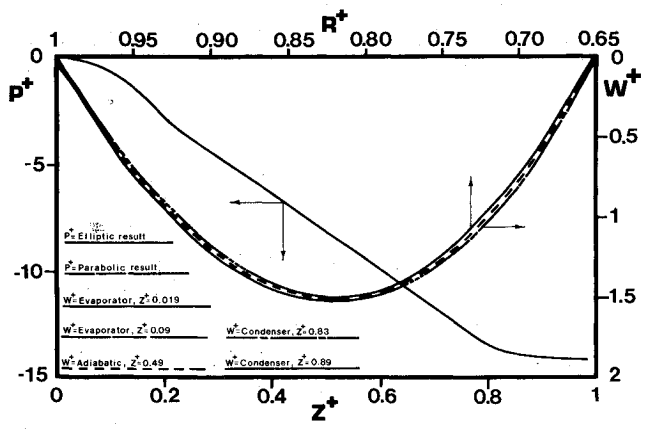

Fig. 5 Comparison of the elliptic and parabolic normalized pressure drop and radial variation of the normalized axial velocity along the heat pipe with $K = 0.65$ evaporator Re, at both walls = 4.0, condenser Re, at both walls = 4.0.

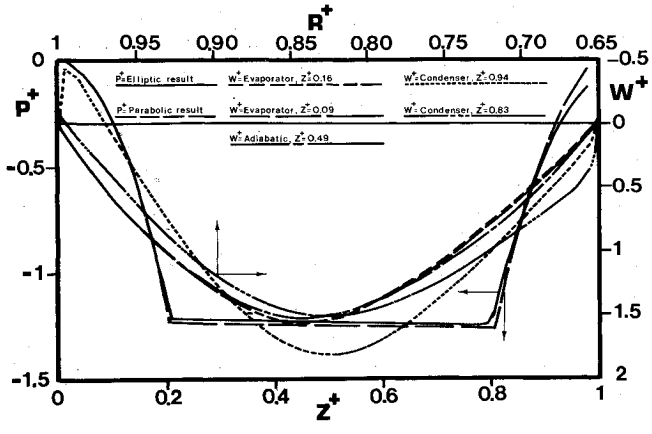

Fig. 6 Comparison of the elliptic and parabolic normalized pressure drop and radial variation of the normalized axial velocity along the heat pipe with $K = 0.65$ evaporator Re at both walls = 1000, condenser Re, at both walls = 1000.

numbers at the inner and outer walls were 1000. In this case, there is a rapid pressure drop in the evaporator section caused by the increase in the axial momentum of the flow, while the pressure stays nearly constant throughout the adiabatic section. The pressure increases, however, along the condenser section in the direction of the flow as a consequence of partial dynamic recovery in the decelerating flow. The pressure drop profiles in the evaporator and condenser sections demonstrate the effects of the pressure head absorbed or created by evaporation and condensation.

A comparison between the normalized pressure drop profiles obtained by the elliptic and the partially parabolic methods for case 3 is made in Fig. 6. The numerical results obtained by the partially parabolic method are within 1.8% of those obtained by the elliptic method. Therefore, it is valid to assume that the boundary-layer method results in a good approximation of numerical results for the cases with high radial Reynolds numbers.

The radial profiles of the axial velocity for case 3 are also presented at five different axial locations in Fig. 6. In this case, the axial velocity profile stays parabolic through the evaporator and adiabatic sections. In the evaporator, the axial velocity gradients are nearly zero, which indicates that the flow becomes fully developed at approximately $Z^+ = 0.09$. The same fully developed profile is observed in the adiabatic section. As the flow proceeds into the condenser section, however, there is a continuous change in the shape of the axial velocity profile. Moreover, there is a region where the flow reverses close to the end of the outer wall in the condenser section. This may be due to the failure of the fluid to possess sufficient momentum to overcome the pressure rise between the condenser inlet and the point where the fluid is withdrawn from the pipe. When the flow reverses in the condenser section, the similarity of the axial velocity profile along the annulus disappears for the cases with high radial Reynolds numbers in the condenser section.

Figure 7 presents the axial pressure drop distribution along the centerline of the heat pipe under the heating and cooling conditions of cases 4-6. In case 4, the blowing velocities at both the inner and outer walls of the evaporator section are the same. Note that this does not correspond to a symmetrical heating condition. Because of the particular geometry, the radial Reynolds number at the outer wall is greater than the radial Reynolds number at the inner wall. The normalized pressure drop along the evaporator and adiabatic sections are identical to case 3. However, in case 4, the pressure recovery in the condenser section does not increase as much as that in case 3. Note that, in case 4, the suction velocities at both walls in the condenser section are higher than those of case 3.

In case 5, the condensation process takes place under the same suction velocities at both walls. The normalized axial pressure drop in the evaporator and adiabatic sections under the conditions of case 5 are identical to the drop observed under the conditions of case 3. As in case 4, the pressure recovery observed in the condenser in case 5 is not as large as that for case 3. In case 5, the flow reverses all along the condenser section, but the flow does not reverse as much as in case 4 because of the lower suction velocities of case 5 compared to case 4.

The pressure drops observed along the evaporator and adiabatic secdtion of case 6 are also identical to those observed in case 3. However, the pressure recovery in the condenser section does not increase as much as that in case 3.

It is obvious that the flow reverses in the condenser section at high radial Reynolds numbers. The normalized axial velocity profiles of the cases with high radial Reynolds numbers also indicate that the axial velocity profile in the condenser section changes with increasing axial distance. This emphasizes the disappearance of similar flows for the cases with very high cooling rates.

Fully Developed Approximation

It is the objective of this section to provide an analytical method to predict the pressure drop along the double-walled annular heat pipe because the numerical solution of the full governing equations is laborious and requires a large amount of computer time. From the previous numerical analysis, one can generalize that the vapor flow in an annular heat pipe becomes fully developed in a very short distance from the evaporator end cap and that this similar profile repeats itself in the adiabatic and condenser sections for low and moderate radial Reynolds numbers, as well as when the walls are impermeable. This entry distance is not significant in many practical applications, as shown in the previous section. The criterion for the fully developed flow is that the dimensionless axial velocity $w/w_{z,m}$ is invariant along the pipe. One very interesting feature of the numerical results presented was that W^+ was similar for various radial Reynolds numbers, including the one with zero inner and outer radial Reynolds numbers. The fully developed normalized velocity profile for annular flow for zero blowing velocity can be easily obtained analytically.[19]

$$W^+ = \frac{w}{w_{zm}} = \frac{w^*}{w^*_{z,m}} = \frac{2\left[1 - R^{+2} + \left(\frac{1-K^2}{\ell n\ 1/K}\right)\ell n(R^+)\right]}{(1-K^4)/(1-K^2)] - [(1-K^2)/(\ell n\ 1/K)]} \tag{6}$$

Table 1 Blowing and suction velocities corresponding to cases in which the double-walled annular heat pipe was studied

Case no.	$V_{I,E}$, m/s $Re_{I,E}$	$V_{O,E}$, m/s $Re_{O,E}$	$V_{I,C}$, m/s $Re_{I,E}$	$V_{O,C}$, m/s $Re_{O,C}$	Axial Reynolds no., $Re_z(z=\frac{LT}{2})$
1	1.45E-5 0.01	-0.947E-5 0.01	-1.45E5 0.01	0.947E-5 0.01	0.4242
2	5.810E-3 4.0	-3.78E-3 4.0	-5.81E-3 4.0	3.78E-3 4.0	169.7
3	1.45 1000	-0.947 1000	-1.45 1000	0.947 1000	42,422.0
4	1.45 1000	-1.45 1530	-2.08 1430	1.04 1100	53,714.0
5	0.725 500	-1.45 1530	-1.45 800	1.16 1230	42,966.0
6	0.725 500	-1.45 1530	-1.67 1150	0.835 900	43,121.0

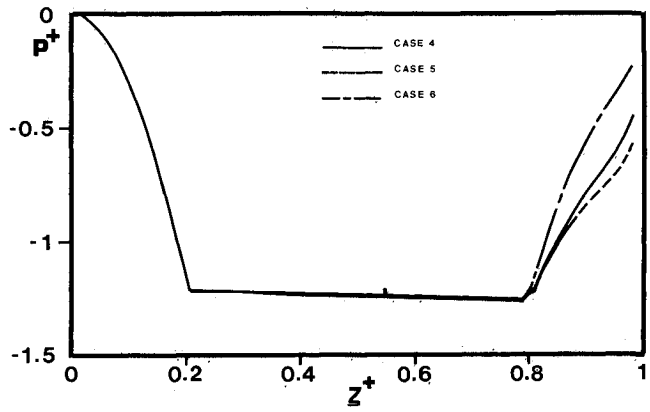

Fig. 7 Normalized pressure distribution along the centerline of the heat pipe with $K = 0.6$ for cases 4–6.

The dimensionless local mean axial velocity $w^*_{z,m}$ can be obtained by making a mass balance in the evaporator section of the heat pipe.

$$w^*_{z,m} = \frac{2(Re_{I,E} + |Re_{O,E}|)z^*}{1-K^2} \tag{7}$$

According to the numerical results discussed in the previous section, Eq. (6) also presents the normalized velocity W^+ for all of the radial Reynolds numbers and K values in the fully developed region.

Assuming an incompressible fluid, constant and normal injection velocities along the length of the pipe wall, and constant pressure along the radius of the pipe, the system of equations in dimensionless form describing the vapor flow is reduced to the following forms:

$$w^*\frac{\partial w^*}{\partial z^*} + v^*\frac{\partial w^*}{\partial R^+} = -\frac{\partial P^+}{\partial z^*} + \frac{1}{R^+}\frac{\partial}{\partial R^+}\left(R^+\frac{\partial w^*}{\partial R^+}\right) \tag{8}$$

$$R^+\frac{\partial w^*}{\partial z^*} + \frac{\partial (v^* R^+)}{\partial R^+} = 0 \tag{9}$$

The boundary conditions appropriate for the evaporator section are as follows:

$$v^*(R^+,0) = w^*(R^+,0) = 0$$

$$w^*(K,z^*) = w^*(1,z^*) = 0$$

$$v^*(K,z^*) = \frac{RO\ V_{I,E}}{\nu} = \frac{Re_{I,E}}{K}$$

$$v^*(1,z^*) = \frac{RO\ V_{O,E}}{\nu} = Re_{O,E} \tag{10}$$

The systems of Eq. (8) and (9) are reduced to the following form by the elimination of the radial velocity in the evaporator section:

$$w^*\frac{\partial w^*}{\partial z^*} + \left[\frac{RE_{I,E}}{R^+} - \frac{1}{R^+}\int_K^{R^+} R^+\frac{\partial w^*}{\partial z^*}\,dR^+\right] \times \frac{\partial w^*}{\partial R^+} = -\frac{\partial P^+}{\partial z^*} + \frac{1}{R^+}\frac{\partial}{\partial R^+}\left(R^+\frac{\partial w^*}{\partial R^+}\right) \tag{11}$$

The pressure drop is obtained by substituting expression (6) into the following integral equation:

$$\int_K^1 w^*\frac{\partial w^*}{\partial z^*}R^+\,dR^+ - \int_K^1\left[\frac{\partial w^*}{\partial R^+}\int_K^{R^+}\left(R^+\frac{\partial w^*}{\partial z^*}\right)dR^+\right] dR^+ = -\frac{\partial P^+}{\partial z^*}\left(\frac{1}{2}-\frac{K^2}{2}\right) + \left(R^+\frac{\partial W^*}{\partial R^+}\right)_K^1 \tag{12}$$

The pressure drop along the evaporator section of the double-walled annular heat pipe is calculated using the following expression:

$$P_E^{\pm} = \frac{2}{K^2-1}\left\{Cz^{*2}(1-K^2) + \frac{C^2z^{*2}}{2}\left[\frac{1}{3} - \frac{3}{4}A + \frac{A^2}{2} - K^2 + K^4 - 2AK^2\ell nK + AK^2 - \frac{K^6}{3} + AK^4\ell nK - \frac{AK^4}{4} - A^2K^2(\ell nK)^2 + A^2K^2\ell nK - \frac{A^2K^2}{2}\right]\right\} \tag{13}$$

A comparison can be made for the prediction of the pressure using the Eq. (13) with the previous numerical results for $Re_{I,E} = 1.5$, $Re_{O,E} = -3.0$, and $K = 0.5$. At $z^* = 0.05$, ex-

pression (13) predicts the pressure within 7% and at $z^* = 0.2$ within 1% of the numerical results.

A similarity expression can be obtained for the pressure in the condenser section by using the appropriate form for $w^*_{z,m}$ in Eq. (6). The following expression for $w^*_{z,m}$ is obtained by a mass balance in the condenser zone:

$$w^*_{z,m} = 1 - \frac{2(|Re_{I,C}| + Re_{O,C})z^*}{(1 - K^2)} \tag{14}$$

The pressure drop in the condenser segment using the parabolic profile is given by

$$P_C^{\pm} = 4[(K^2 - 1 + C' \cdot E)/(K^2 - 1)][(C'z^{*2}/2 - Dz^*] \tag{15}$$

where E is

$$E = \left\{\frac{1}{6} - \frac{3A}{8} + \frac{A^2}{4} - \frac{K^2}{2} + \frac{K^4}{2} - \frac{K^6}{6} - AK^2 \ell nK + \frac{AK^2}{2} + \frac{(AK^4 \ell nK)}{2} - \frac{AK^4}{8} - \frac{A^2K^2(\ell nK)^2}{2} + \frac{A^2K^2 \ell nK}{2} - \frac{A^2K^2}{4}\right\} \tag{16}$$

It should be noted that by using w^* given by the product (6) and (14), one can also predict where the flow reverses in the condenser section. When the flow reverses, $w^*_{z,m}$ and w^* are both negative, and the ratio $w^*/w^*_{z,m}$ is still given by expression (6) in this segment. A prediction of the pressure by expression (15) in the condenser zone before the flow reverses for $Re_{I,C} = -1.5$, $Re_{O,C} = 3.0$, and $K = 0.5$ at $z^* = 0.03$ and $z^* = 0.05$ is within 1 and 8% of the previous numerical results, respectively. It is interesting to note that expression (14) can predict the location at which the flow reverses at various condensation rates in the condenser zone by having negative $w^*_{z,m}$. This gives the location at which the flow reverses to be $z_R \cong 0.11$ for the preceding condenser specifications. Expression (15) can also be used to calculate accurately the pressure drop in the adiabatic section.

Conclusions

The results of the investigation warrant the following conclusions:

1) Accurate prediction of the pressure loss can be made all along the double-walled annular heat pipe by using the fully parabolic version of the equations of motion and solving different segments of the heat pipe independently of each other. This can be achieved by letting the inlet velocity be zero in the evaporator zone and the axial velocity have a parabolic inlet profile for the adiabatic and condenser sections.
2) For laminar vapor flows in double-walled annular heat pipes, the flow in the condenser may exhibit a region where the axial velocity reverses when the condenser radial Reynolds numbers are high.
3) The hydrodynamic entry length for the evaporator section is very short and can be neglected in many practical applications. This justifies the use of a similarity velocity profile (6) all along the evaporator section.
4) The normalized velocity distribution W^+ given by expression (6) can be used all along the double-walled annular heat pipe for radial Reynolds numbers at the inner and outer walls up to 4.0.
5) Accurate estimates of the overall pressure loss may be made by using Eqs. (13) and (15).

Acknowledgments

Funding for this work was provided by the Thermal Energy Group of the Aeropropulsion Laboratory of the Air Force Wright Aeronautical Laboratories under Contract F-33615-81-C-2012. The authors are indebted to Dr. E.T. Mahefkey and Dr. J.E. Beam for technical consultation on this project.

References

[1]Levy, E.K., "Theoretical Investigation of Heat Pipes Operating at Low Vapor Pressure," *Journal of Engineering for Industry,* Vol. 90, Series B, Nov. 1968, pp. 547-552.

[2]Hornbeck, R.W. Rauleau, W.T. and Osterle, F., "Laminar Entry Problem in Porous Tubes," *Physics of Fluids,* Vol. 6, Nov. 1963.

[3]Busse, C.A., "Pressure Drop in the Vapor Phase of Long Heat Pipes," *1967 IEEE Conference Record of the Thermionic Conversion Specialist Conference,* Palo Alto, CA, 1967, pp. 391-398.

[4]Weissberg, H.L. "Laminar Flow in the Entrance Region of a Porous Pipe," *Physics of Fluids,* Vol. 2, Sept. 1959.

[5]Terrill, R.M. and Thomas, P.W., "On Laminar Flow Through a Uniformly Porous Pipe," *Applied Science Research,* Vol. 21, Aug. 1969.

[6]Knight, B.W. and McInteer, B.B., "Laminar Incompressible Flow in Channels with Porous Walls," Los Alamos Scientific Laboratory, Los Alamos, NM, LADC-5039, 1965.

[7]Yuan, S.W. and Findelstein, A.B., "Laminar Flow with Injection and Suction Through a Porous Wall," *Proceedings of the Heat Transfer and Fluid Mechanics Institute,* Los Angeles, CA, 1955.

[8]Bankston, C.A. and Smith, H.J., "Vapor Flow in Cylindrical Heat Pipes," *Journal of Heat Transfer,* Vol. 95, 1973, pp. 371-376.

[9]Quile, J.P. and Levy, E.K., "Laminar Flow in a Porous Tube with Suction," ASME Paper 73-WA/HT-1, 1973.

[10]Tien, C.L. and Rohani, A.R., "Analysis of the Effects of Vapor Pressure Drop on Heat Pipe Performance," *International Journal of Heat and Mass Transfer,* Vol. 17, 1974, pp. 61-67.

[11]Busse, C.A. and Prenger, F.C., "Numerical Analysis of the Vapor Flow in Cylindrical Heat Pipes," *Proceedings of the Fifth International Heat Pipe Conference,* Tsukuba Science City, Japan, May 1984.

[12]Faghri, A., "Vapor Flow Analysis in a Double-Walled Concentric Heat Pipe," *Numerical Heat Transfer,* Vol. 12, Dec. 1986, pp. 583-595.

[13]Faghri, A., "Performance Characteristics of the Double-Walled Concentric Heat Pipe," *Proceedings of the Sixth International Heat Pipe Conference,* France, May 1987.

[14]Spalding, D.B., "A General Purpose Computer Program for Multi-Dimensional One- and Two-Phase Flow," *Mathematics and Computers in Simulation,* Vol. XXIII, North Holland, Amsterdam, the Netherlands, 1981, pp. 267-276.

[15]Spalding, D.B., "Mathematical Modeling of Fluid Mechanics, Heat Transfer and Chemical-Reaction Processes," A Lecture Course, CFDU Report, HTS/80/1, Imperial College, London, 1980.

[16]Spalding, D.B. and Rosten, H.I., *PHOENICS-Beginner's Guide,* CHAM Lt., Dec. 1985.

[17]Patankar, S.V., *Numerical Heat Transfer and Fluid Flow,* Hemisphere, 1980.

[18]Parvani, S., "Numerical Analysis of Vapor Flow in a Double-Walled Concentric Heat Pipe," M.S. Dissertation, Wright State University, Dayton, OH, 1986.

[19]Langhaar, H.L., "Steady Flow in the Transition Length of a Straight Tube", *Journal of Applied Mechanics,* Vol. 9, 1942, pp. A55-A58.